Lidar observations of atmospheric internal waves in the boundary layer of atmosphere on the coast of Lake Baikal

Viktor A. Banakh, Igor N. Smalikho

V.E. Zuev Institute of Atmospheric Optics SB RAS, Tomsk, Russia

Correspondence to: V.A. Banakh (banakh@iao.ru)

Abstract. Atmospheric internal waves (AIWs) in the boundary layer of atmosphere have been studied experimentally with the use of Halo Photonics pulsed coherent Doppler wind lidar Stream Line. The measurements were carried out in August 14-28 of 2015 on the western coast of Lake Baikal (51°50'47.17"N, 104°53'31.21"E), Russia. The lidar placed at a distance of 340 m from Lake Baikal at a height of 180 m above the lake level.

A total of six AIW occurrences have been revealed. This always happened in the presence of one or two (in 5 of 6 cases) narrow jet streams at heights of approximately 200 and 700 m above ground level at the lidar location. The period of oscillations of the wave addend of the wind velocity components in four AIW events was 9 min, and in two other it was approximately 18 and 6.5 min. The amplitude of oscillations of the horizontal wind velocity component was about 1 m/s, while the amplitude of oscillations of the vertical velocity was three times less. In the most cases, internal waves were observed for 45 min (5 wave oscillations with a period of 9 min). Only one time the AIW lifetime was about four hours.

1 Introduction

Atmospheric gravity waves (AGWs) are an important feature of motions present in the atmosphere. They are responsible for transfer of addititious mechanic and thermal energy, which leads to the spatial inhomogeneity and temporal variability of the wind and temperature fields. As AGWs destroy, the released energy causes turbulization of the wind and temperature fields. Detail review of works in this subject was done recently by Plougonven and Zhang, 2014 and by Sun et al., 2015.

Study of the gravity waves is carried out with the help of space images of the cloud fields in the visible and microwave regions [for example, (German, 1985; Li et al., 2001)] and radar images of the sea surface [for example, (Spiridonov et al., 1987; Chunchuzov et al., 2000)]. Experimental investigations of AGWs in the ionosphere from the scattering of radio waves are carried out by different methods [for example, (Benediktov et al., 1997)]. The first results of lidar observations of the inertnal gravity waves in the stratosphere and mesosphere with the use of the Doppler Rayleigh lidar are reported in (Baumgarten et al., 2015). An airborne 2-μm CDWL was used by Chousa et al. (2016) for research of island induced gravity waves.

AGW observations in the lower atmosphere, in particular, in the atmospheric boundary layer (ABL) are based mostly on fixed-point or mobile platform pressure measurements (Román-Cascón et al., 2015, Sun et al., 2015). For study of AGW, coherent Doppler wind lidars (CDWLs) and sodars are used as well. Newsom and Banta (2003) and Wang et al. (2013) applied 2-μm CDWL for investigation of low-level jet and gravity waves in the stable ABL over a flat and urban terrain, respectively. Lyulyukin et al. (2015) observed AGW in the atmospheric lower 300-400 m layer based on sodar data. However, the data of lidar and sodar observations of AGW in the ABL are few and far between.

In this paper we present the results of lidar observations of the coastal-mountain lee waves on the coast of Lake Baikal. Lee AIWs (or orographic waves) are one of the types of AGWs, which arise on leeward of obstacles at the stable stratification of an incoming flow (Vel'tishchev and Stepanenko, 2006; Kozhevnikov, 1999). Experimental investigations of AIWs in the atmospheric boundary layer of Lake Baikal were carried out with the use of the 1.5 μm Halo Photonics CDWL Stream Line (Pearson, 2009). These lidars find expanding applications in studies of ABL (O'Connor et al., 2010, Sathe and Mann, 2012; Dinther et al., 2015; Päschke et al., 2015; Smalikho and Banakh, 2015a,b; Smalikho et al., 2015 a,b,c; Vakkari et al., 2015).

The processing of all data measured by the lidar and analysis of the processed data have revealed several cases of formation of atmospheric internal waves for the period of measurements. Formation of one and often simultaneously two narrow jet streams at heights of the atmospheric boundary layer were observed as well. In all the cases, AIWs were formed in the presence of low-level jet streams.

2 Lidar, measurement strategy, and data processing

The main parameters of lidar Stream Line used in the experiment on the shore of Lake Baikal are given in Table 1. Despite of the low energy of the probing pulse, relatively high pulse repetition frequency f_P allows one to use for accumulation of raw lidar data a large number of laser shots N_a and obtain estimation of radial velocity with required accuracy and time resolution.

Measurement strategy of this lidar was as follows. During the experiment we used the conical scanning (see Figure 1). At fixed elevation angle φ the probing laser beam was rotated continuously around the vertical axis Z with the angular speed $\omega_s = 2\pi / T_{\text{scan}}$, where T_{scan} is the duration of one full scan, starting from the azimuth angle $\theta = 0°$ to $\theta = 360°$. Then, the laser beam was stopped and after 0.3 seconds it began a continuous rotation in the opposite direction to the angle $\theta = 0°$. After 0.3 seconds the cycle repeated. The above procedure executed continuously during the experiment.

For lidar observation of the atmospheric gravity waves in the atmospheric boundary layer, the scan time T_{scan} and the diameter of the scan cone base should be set as small as possible. The scan cone base diameter $d = 2R\cos\varphi$ at the distance R from the lidar depends on the beam elevation angle φ. With $\varphi \to 90°$ (for decreasing the scan cone base) the error of estimation of horizontal components of the wind vector $\mathbf{V} = \{V_z, V_x, V_y\}$, where V_Z is the vertical component, increases

indefinitely due to wind turbulence and random instrumental errors of estimation of the radial velocity V_r. The lower the signal-to-noise ratio SNR (ratio of the mean signal power to the mean noise power for fixed range R), the greater the increase in error. In our experiment, we set the elevation angle $\varphi = 60°$ at which the height above the lidar $h = d$.

Taking into account that the typical period of the atmospheric gravity wave is, at least, several minutes, we set T_{scan} = 36 seconds. At N_a = 3000 (measurement duration $T_{\text{ray}} = N_a / f_P$ = 0.2 s), after data preprocessing by the lidar internal PC, for one full scan we have arrays of estimates of the radial velocity $\hat{V}_r(R_k, \theta_m)$ and the signal-to-noise ratio $\hat{\text{SNR}}(R_k, \theta_m)$ for $M = T_{\text{scan}} / T_{\text{ray}}$ = 180 rays, where $R_k = R_0 + k\Delta R$ is the current range, R_0 = 105 m, $k = 0, 1, 2, 3, ..., K-1$, K = 63, ΔR = 30 m, θ_m is the azimuth angle, $m = 1, 2, 3, ..., M$ (ideally, for increasing angle $\theta_m = m\Delta\theta$ and $\Delta\theta$ = 2°). The range R_k corresponds to the height above ground level (AGL) $h_k = R_k \sin\varphi$. All measurement parameters are given in Table 2.

From the array $\hat{V}_r(R_k, \theta_m)$ measured at φ = 60° and relatively high SNR (when probability of "bad" (unreliable) estimate of the radial velocity is very small)) one can obtain acceptable estimate of the wind vector $\hat{\mathbf{V}} = \{\hat{V}_z, \hat{V}_x, \hat{V}_y\}$, using the fitting of $\mathbf{S}(\theta_m) \cdot \mathbf{V}$, where $\mathbf{S}(\theta_m) = \{\sin\varphi, \cos\varphi\cos\theta_m, \cos\varphi\sin\theta_m\}$, to the array $\hat{V}_r(R_k, \theta_m)$ by the least square method (LSM). To judge the acceptability of this estimate, it is necessary to know the threshold signal-to-noise ratio SNR_t that depends, in particular, on N_a.

To obtain the results represented in Section 3, we used the filtered sine-wave fitting (FSWF) (Smalikho, 2003; Banakh et al., 2009; Banakh and Smalikho, 2013; Banakh et al., 2015). This method is based on finding the maximum of the function

$$Q(\mathbf{V}) = \sum_{m=1}^{M} \exp\{-[\hat{V}_r(R_k, \theta_m) - \mathbf{S}(\theta_m) \cdot \mathbf{V}]^2 / (2\sigma^2)\}, \quad (1)$$

where σ is the filtration parameter (we set σ = 2 m/s), that is, $\max\{Q(\mathbf{V})\} = Q(\hat{\mathbf{V}})$ at each height h_k sequentially. In contrast to the LSM, the FSWF filters "good" (reliable) estimates $\hat{V}_r(R_k, \theta_m)$, when $\hat{\mathbf{V}}$ is true, at very low SNR. At high SNR and correctly chosen $\sigma \geq$ 2 m/s, the LSM and FSWF give similar results even in the case of strong wind turbulence. From the estimate of wind velocity vector $\hat{\mathbf{V}}$ the horizontal wind velocity U and the wind direction angle θ_V are calculated.

Figure 2 shows an example of wind profiles $U(h_k)$, $\theta_V(h_k)$ и $\hat{V}_z(h_k)$ retrieved from data measured by the Stream Line lidar on the shore of Lake Baikal, August 25, 2015 at 23:15:30 local time (here and in other figures the height is above the lidar position level). For retrieval of wind profiles in Fig.2 we used both LSM and FSWF methods. The figure shows also the profile of estimate of the signal-to-noise ratio obtained from the same measurement and averaged over all the rays: $\bar{\text{SNR}}(h_k) = M^{-1} \sum_{m=1}^{M} \hat{\text{SNR}}(R_k, \theta_m)$. It is seen from the figure that both these methods give similar results, except for a layer of

600-900 m and over 1400 m. Due to the filtration of data, the FSWF provides more smooth profiles of the wind in the layers 600-900 m and 1400-1500 m than the LSM. That proves a greater effectiveness of the FSWF as compared to the LSM.

The mean noise power is a function of the range R (Manninger et al., 2016). Therefore, at very low signal-to-noise ratios the estimate $\overline{\mathrm{SNR}}(h_k)$ has systematic error (in particular, $\overline{\mathrm{SNR}}$ can take negative values). That does not allow the finding of adequate threshold SNR_t without special procedure of data correction (Manninger et al., 2016). For the correction of measured profile $\overline{\mathrm{SNR}}(h_k)$ first, we use a smoothing cubic spline fit to all $\overline{\mathrm{SNR}}(h_k) \le 0.015$ and obtain the function $\mathrm{SNR}_s(h_k)$ (see green squares in Figure 2(d)). Then, assuming that at some heights h_k, the true SNR is very close to zero, we find the minimum of the function $\mathrm{SNR}_s(h_k)$ and obtain a corrected profile of the signal-to-noise ratio in the form:

$$\mathrm{SNR}_c(h_k) = \mathrm{SNR}_s(h_k) - \min\{\mathrm{SNR}_s(h_k)\} + \mathrm{SNR}_{\min}, \quad (2)$$

where $\mathrm{SNR}_{\min}$ is unknown true minimal SNR. We note that in practice the heights of $\min\{\mathrm{SNR}_s(h_k)\}$ and $\mathrm{SNR}_{\min}$ can be different.

To avoid the necessity of determination of $\mathrm{SNR}_{\min}$ we proceeded as follows. From our measurement by the Stream Line lidar in Tomsk in September of 2015 (focus length was 300 m; the measurements were carried out in clear weather without clouds), using the raw data (in binary files for correlation functions of the complex lidar signal) we obtained the following function

$$N(R) = [P_N(R) - \bar{P}_N] / \bar{P}_N, \quad (3)$$

where $P_N(R)$ is the mean noise power as function of range R and $\bar{P}_N$ is the noise power averaged over interval from 1 km to 3 km. Example of the function *N(R)* is shown in Figure 3. According to the figure, in the interval 1-2 km the function $N(R)$ has regular oscillation with amplitude $A \sim 0.001$ and range period $L \sim 450$ m (at elevation angle $\varphi = 60°$ the height period $L\sin\varphi \sim 400$ m).

Let us assume that $\mathrm{SNR}_{\min} = 0.001$. The result of calculation by Eq. (2) at $\mathrm{SNR}_{\min} = 0.001$ (-30 dB) is shown in Figure 2(d) as green solid curve. If assumption $\mathrm{SNR}_{\min} = 0.001$ is correct, then the threshold signal-to-noise ratios can be set as $\mathrm{SNR}_t = 0.005$ (-23 dB) in the case of FSWF and $\mathrm{SNR}_t = 0.01$ (-20 dB) in the case of LSM. These thresholds are found from the profiles shown in Figure 2(a-c) and depicted in Figure 2(d) as blue and red lines, respectively. In the paper of Päschke at al. (2015) the authors assert that the decrease of the threshold SNR from 0.015 down to 0.01 would increase the data availability by almost 40 %. It corresponds to the LSM profiles presented in Figure 2(a-c). Since in the experiments on Lake Baikal for processing the data we used the FSWF, then we could use as SNR threshold the value $\mathrm{SNR}_t = 0.005 - \mathrm{SNR}_{\min} = 0.005 - 0.001 = 0.004$. Taking into account that regular oscillations of SNR of our lidar have maximal amplitude about $A \sim 0.001$ (Fig.3), upon obtaining the results presented below, we rejected the wind estimates that do not satisfy the condition

$$\mathrm{SNR}_s(h_k) - \min\{\mathrm{SNR}_s(h_k)\} \geq 0.005, \quad (4)$$

where information about $\mathrm{SNR}_{\min}$ is not required. In color figures of this paper the rejected estimates are shown in black.

3 Observations and analysis

The measurements were conducted in August 14-28 of 2015 on the western coast of Lake Baikal (51°50'47.17"N, 104°53'31.21"E) at the territory of Baikal Astrophysical Observatory of the Institute of Solar-Terrestrial Physics SB RAS, near the Baikal Solar Vacuum Telescope (BSVT). The lidar was set at a minimum distance of 340 m from Baikal at a height of 180 m above the lake level (see Fig. 4). According to Google map, the profile of the relief surface of the earth starting from position of the lidar in direction to North up to 30 km from the lidar has 10 local maxima with heights of 180 – 420 m and the same number of minimums with heights of 60 – 250 m above Lake Baikal level. Due to forest fires, the atmosphere often contained greater amounts of aerosol, and, correspondingly, the lidar signal-to-noise ratio was rather high.

Figure 5 shows the results of lidar visualization of the wind field during the longest observations of a gravity wave for about 4 hours starting from 12:00 Local Time on August 23 of 2015. Two jet streams were observed simultaneously at heights of about 250 and 750 m AGL. Direction of first jet stream (at height of 250 m) was from North to South and direction of the other one was from East to West.

Figures 6 and 7 show the vertical profiles at 14:31 LT and temporal profiles at a height of 636.5 m AGL of wind taken from data in Fig. 5. From these figures, we can clearly see oscillations of the wind speed, direction, and vertical component in both height and time. They are especially evident in the period from 13:30 to 15:30 LT, when the amplitude of oscillations of the wind direction is maximal and equal to approximately 45°.

Neglecting the wind turbulence, we use the model of a plane wave for the component of the wind velocity vector V_α (subscript $\alpha = z$ for the vertical component, $\alpha = x$ for the longitudinal component, and $\alpha = y$ for the transverse component) in the form (Vinnichenko et al., 1973)

$$V_\alpha(\mathbf{r},t) = <V_\alpha> + \tilde{V}_\alpha(\mathbf{r},t). \quad (5)$$

In Eq.(5) $\mathbf{r} = \{z, x, y\}$ is the radius vector in the Cartesian system of coordinates with center at point of the lidar position, t is time, $<V_\alpha>$ and $\tilde{V}_\alpha$ are the regular and wave addends of the α -th component of the wind velocity, respectively,

$$\tilde{V}_\alpha(\mathbf{r},t) = A_\alpha(z)\sin\left[\psi_\alpha(\mathbf{r}) - 2\pi t / T_v\right], \quad (6)$$

A_α is the wave amplitude, ψ_α is the wave phase, and T_v is the wave period. If the wind direction coincides with the direction of propagation of the internal gravity wave, then $A_y = 0$, $\psi_x = 2\pi x / \lambda_v$, and $\psi_z = 2\pi x / \lambda_v + \pi / 2$ (Vinnichenko et al., 1973). Here, λ_v is the wavelength of the wave propagating with the speed $c_v = \lambda_v / T_v$.

Models (5) and (6) were applied in the analysis of data in Fig.5 for a height of 766.4 m AGL (inside the upper jet stream) and 47-min time interval starting from 14:20 LT, when the amplitude of wind velocity oscillations was maximal. From these data, with allowance made for the linear trend, we found the wave addends $\tilde{V}_\alpha(\mathbf{r},t)$ for the three components of the wind velocity vector. In Fig. 8, the solid curve shows the dependence of $\tilde{V}_x$ on t. To determine the wave frequency $f_v = 1/T_v$, we have used experimental function $\tilde{V}_x(t)$ and calculated the spectral density, which is depicted in Fig.9. The obtained spectrum has a peak, from whose position we have determined the frequency f_v to be equal to 0.00185 Hz. Consequently, the wave period is T_v = 9 min. Using the least-square fitting of model (6) for $\tilde{V}_x(t)$ to the wave addend of the wind velocity component measured by the lidar (solid curve in Fig. 8), we have determined the phase ψ_x and the amplitude A_x. The amplitude of wave addend for the longitudinal component of the wind velocity vector turned out to be 0.96 m/s. The model temporal profile $\tilde{V}_x(t)$ calculated by Eq. (6) with the use of experimental values of A_x, ψ_x, and T_v is shown as a dashed curve in Fig. 8.

Parameters of the wave addend of the vertical wind velocity $\tilde{V}_z(t)$ were found in the same way. The estimates of periods of the internal wave for the longitudinal and vertical components coincided fully (T_v = 9 min), amplitude A_z = 0.3 m/s is approximately 3 times less than the amplitude of wave addend of the longitudinal component of the wind velocity vector, and $\psi_z - \psi_x = \pi/2$. Since the amplitude $A_y \neq 0$ (see Fig. 5(b) and Fig. 7(b)), the direction of propagation of the internal wave did not coincide with the wind direction.

To estimate the wind turbulence strength during observation of the AIW, we used the array of radial velocities measured from 14:20 to 15:20 LT on August 23 of 2015 and retrieved a vertical profile of the turbulent energy dissipation rate ε in the layer 200-500 m AGL by the method described in paper of Smalikho et al. (2015c). Obtained values ε are rather small and decreases with height from $3\cdot10^{-5}$ m^2/s^3 at 200 m to approximately 10^{-5} m^2/s^3 at 500 m. For calculation of contribution of the turbulence into variation of lidar estimates of the wind velocity, it is necessary to know, at least, the integral scale of the longitudinal wind velocity correlation L_l. Unfortunately, the measurement geometry used in the experiment did not allow us to obtain estimation of L_l from the measured lidar data. Due to the filtration (see Section 2) the instrumental error of wind velocity estimate, obtained at M = 180 and SNR threshold 0.005 (Eq. (4)), does not exceed 0.1 m/s. In our experiment for heights h < 500 m AGL it did not exceed 0.05 m/s usually). For the vertical wind component the instrumental error is approximately 3 times less.

Figures 5-7 illustrate the long time AIW in the case of weak wind, when wind velocity averaged over period T_v is 1 – 2.5 m/s. Figure 10(a) shows an example of the spatiotemporal distribution of wind velocity, where the atmospheric internal wave was observed since 5:30 LT for about 40 min, when the averaged wind velocity was about 5.5 m/s. According to the data of

Fig. 10(b), the period and amplitude of the wave were, respectively, 9 min and 0.9 m/s. Two jet streams were also observed for 5 hours: one at a height of approximately 200 m AGL, and another at a height of 500 m AGL and higher.

Figure 11 depicts the spatiotemporal distributions of wind and the signal-to-noise ratio in the evening of August 14 for about 45 min. Here we see one jet stream at a height ~730 m AGL and an atmospheric internal wave. In the layer of 100-500 m AGL, the oscillations of the wind speed, direction, and vertical component are accompanied by periodic variations of the signal-to-noise ratio SNR. It is known that SNR is proportional to the aerosol backscatter coefficient β_π. For range $R \le 250$ m effect of turbulent pulsations of the refractive index of air on the intensity of the laser beam focused at distance of 800 m (see Table 2) can be neglected. Therefore for such ranges the SNR also does not depend on turbulent pulsations of the refractive index. We used the data of Fig. 11(d) for a height of 220.8 m AGL and calculated the relative variations of the backscatter coefficient $\eta(t) = [\beta_\pi(t) - <\beta_\pi>_T]/<\beta_\pi>_T$, as

$$\eta(t) = [\bar{\mathrm{SNR}}(t) - <\bar{\mathrm{SNR}}>_T]/<\bar{\mathrm{SNR}}>_T, \quad (7)$$

where the operator $<...>_T$ denotes the time averaging for the period of 45 min.

Since the SNR oscillates within the height (AGL) range 100-500 m in Fig. 11(d), it is evident, that aerosol backscatter coefficient should vary with time too. These aerosol backscatter coefficient (SNR) variations can be caused by oscillations of the vertical component of the wind velocity vector, whose amplitude is relatively high. To test it, we compared $V_z(t)$ with $\eta(t)$.

Figure 12 shows the temporal profiles $V_z(t)$ and $\eta(t)$ obtained from the data depicted in Fig. 11 for a height of 220.8 m AGL. From the analysis of the curve in Fig.12(a), it follows that the period of oscillations T_v of the vertical component of wind velocity is 6.5 min. The same period of oscillations is also observed for other components of the wind vector, whose phase is shifted by 90° about the phase of $\tilde{V}_z(t)$. According to Fig. 12(b), $\eta(t)$ is characterized not only by periodic variations with time, but also by nonstationarity within the considered time interval. It follows from the rough estimates that the period of oscillations of the aerosol backscatter is close to T_v = 6.5 min, while the phase is shifted from $\tilde{V}_z(t)$ by about 90°.

In addition to these three cases of AIW occurence, we succeeded in observation of this phenomena three times more for the period of measurements. Thus, on August 25 in the predawn time (04:30–05:06 LT), two jet streams and AIW with the period $T_v \approx 9$ min and the amplitude $A_x \approx 1$ m/s at a height of 402.7 m AGL were observed in the atmospheric boundary layer. Next day (August 26 of 2015), the internal wave with the period $T_v \approx 18$ min and the amplitude $A_x \approx 0.7$ m/s at the same height 402.7 m AGL, passed from 16:22 to 19:00 LT. In the same day, the AIW with the halved period ($T_v \approx 9$ min) and the amplitude $A_x \approx 0.4$ m/s at the height 402.7 m AGL was observed 50 min later from 19:50 to 20:35 LT.

3 Summary

Thus, the results of the experimental campaign in the coastal zone of Lake Baikal in August of 2015 show that the raw data of measurements by the Stream Line lidar allow us to visualize the spatiotemporal structure of the wind field in the atmospheric boundary layer and reveal the presence of low-level jet streams and atmospheric internal waves. The distinguishing feature of the atmospheric conditions of the Lake Baikal is occurrence the stable thermal stratification in the ABL during the day time. The low-level jet streams were observed during day and night times while none of the AIWs events were observed in the night time.

A total of six cases of AIW formation have been revealed, which always occurred in presence of one or two (in 5 of 6 cases) narrow jet streams at heights of about 200 and 700 m AGL. When two jet streams were formed, the period of oscillations of the wave addend of the wind vector components was 9 min. In only one case it was about 18 min. In presence of a single jet stream (at a height of 730 m AGL), the period of oscillations of the wind vector components during AIW was about 6.5 min. The amplitude of oscillations of the horizontal wind components most often was about 1 m/s, while the amplitude of oscillations of the vertical velocity was tree times less. In the most cases, the internal waves were observed for 45 min (5 oscillations with the period T_v = 9 min). Only once the lifetime of the atmospheric internal wave was about 4 hours.

Acknowledgments

The authors are thankful to A.V. Falits and A.A. Sukharev for the measurements. The authors are grateful to the Institute of Solar-Terrestrial Physics SB RAS for the possibility of using the territory of the Baikal Observatory for the measurements. This study was supported by the Russian Science Foundation, Project No. 14-17-00386.

References

Banakh, V.A., Brewer, V.A., Pichugina, E.L., Smalikho, I.N.: Measurements of wind velocity and direction with coherent Doppler lidar in conditions of a weak echo signal, Atmos. Oceanic Optics, 23(5), 381-388, doi:10.1134/S1024856010050076, 2010.

Banakh, V. and Smalikho, I.: Coherent Doppler Wind Lidars in a Turbulent Atmosphere, Artech House Publishers, 2013.

Banakh, V.A., Smalikho, I.N., Falits, A.V., Belan, B.D., Arshinov, M.Yu., and Antokhin, P.N.: Joint radiosonde and Doppler lidar measurements of wind in the boundary layer of the atmosphere, Atmos. Oceanic Optics, 28(2), 185-191, doi:10.1134/S1024856015020025, 2015.

Baumgarten, G., Fiedler, J., Hildebrand, J., and Lübken, F.-J.: Inertia gravity wave in the stratosphere and mesosphere observed by Doppler wind and temperature lidar, Geophys, Res. Lett., 42, 10,929–10,936, doi:10.1002/2015GL066991, 2015.

Benediktov, E.A., Belikovich, V.V., Bakhmet'eva, N.V., and Tolmacheva, A.V.: Seasonal and daily variations of the velocity of vertical motions at altitudes of the mesosphere and lower thermosphere near Nizhny Novgorod, Geomagn. Aeron., 37(5), 88-94, 1997.

Chouza, F., Reitebuch, O., Jähn, M., Rahm, S., and Weinzierl, B.: Vertical wind retrieved by airborne lidar and analysis of island induced gravity waves in combination with numerical models and in situ particle measurements, Atmos. Chem. Phys., 16(7), 4675–4692, doi:10.5194/acp-16-4675-2016, 2016.

Chunchuzov, I., Vachon, P., and Li, X.: Analysis and modeling of atmospheric gravity waves observed in Radarsat SAR images, Remote Sens. Environ., 74, 343-361, 2000.

Dinther, D. van, Wood, C.R., Hartogensis, O.K., Nordbo, A., and O'Connor, E.J.: Observing crosswind over urban terrain using scintillometer and Doppler lidar, Atmos. Meas. Tech., 8, 1901–1911, doi:10.5194/amt-8-1901-2015, 2015

German, M.A.: Space Methods of Investigation in Meteorology, Gidrometeoizdat Publishers, 1985 [in Russian].

Kozhevnikov, N.N.: Perturbations of the atmosphere at a flow around mountains, Nauchnyi Mir Publishers, 1999 [in Russian].

Li, X., Zheng Q., Pichel, W.G., Yan, X-H., Liu, W.T., and Clemente-Colon, P.: Analysis of coastal lee waves along the coast of Texas observed in advanced very high resolution radiometer images, Journal of Geophysical Research, 106(C4), 7017-7025, DOI: 10.1029/1999JC000019, 2001.

Lyulyukin, V.S., Kallistratova, M.A., Kouznetsov, R.D., Kuznetsov, D.D., Chunchuzov, I.P., and Chirokova, G.Yu.: Internal gravity-shear waves in the atmospheric boundary layer from acoustic remote sensing data, Izvestiya, Atmospheric and Oceanic Physics., 51(2), 193–202, 2015.

Makarenko, N. I. and Maltseva, J. L.: Interference of lee waves over mountain ranges, Nat. Hazards Earth Syst. Sci., 11(1), 27–32, doi:10.5194/nhess-11-27-2011, 2011.

Manninen, A. J., O'Connor, E. J., Vakkari, V. and Petäjä, T.: A generalised background correction algorithm for a Halo Doppler lidar and its application to data from Finland, Atmos. Meas. Tech., 9(2), 817–827, doi:10.5194/amt-9-817-2016, 2016.

Newsom, R. K. and Banta, R. M.: Shear-flow instability in the stable nocturnal boundary layer as observed by Doppler lidar during CASES-99, J. Atmos. Sci. 60(1), 16–33, 2003.

O'Connor, E. J., Illingworth, A. J., Brooks, I. M., Westbrook, C. D., Hogan, R. J., Davies, F., and Brooks, B. J.: A Method for estimating the turbulent kinetic energy dissipation rate from a vertically pointing Doppler lidar, and independent evaluation from balloon-borne in situ measurements, J. Atmos. Oceanic Technol., 27, 1652–1664, doi:10.1175/2010JTECHA1455.1, 2010.

Päschke, E., Leinweber,R., and Lehmann, V.: An assessment of the performance of a 1.5 μm Doppler lidar for operational vertical wind profiling based on a 1-year trial, Atmos. Meas. Tech., 8, 2251–2266, doi:10.5194/amt-8-2251-2015, 2015.

Pearson, G., Davies, F. and Collier, C.: An Analysis of the Performance of the UFAM Pulsed Doppler Lidar for Observing the Boundary Layer, J. Atmos. Oceanic Technol., 26(2), 240–250, doi:10.1175/2008JTECHA1128.1, 2009.

Plougonven, R. and Zhang, F.: Internal gravity waves from atmospheric jets and fronts, Reviews of Geophysics, 52, 33-76, doi:10.1002/2012RG000419, 2014.

Román-Cascón, C., Yagüe, C., Mahrt, L., Sastre, M., Steeneveld, G.-J., Pardyjak, E., van de Boer, A. and Hartogensis, O.: Interactions among drainage flows, gravity waves and turbulence: a BLLAST case study, Atmos. Chem. Phys., 15(15), 9031–9047, doi:10.5194/acp-15-9031-2015, 2015.

Sathe, A., and Mann,J.: Measurement of turbulence spectra using scanning pulsed wind lidars, J. Geophys. Res., 117, D01201, doi:10.1029/2011JD016786, 10329-10330, 2012.

Smalikho, I.: Techniques of wind vector estimation from data measured with a scanning coherent Doppler lidar, Journal of Atmospheric and Oceanic Technology, 20(2), 276–291, 2003.

Smalikho, I.N., and Banakh V.A.: Estimation of aircraft wake vortex parameters from data measured with a 1.5-μm coherent Doppler lidar, Optics Letters, 40(14), 3408-3411, doi:10.1364/OL.40.003408, 2015a.

Smalikho, I.N., and Banakh V.A.: Estimation of aircraft wake vortex parameters from data measured by a Stream Line lidar, in: Proceedings of SPIE 21st International Symposium "Atmospheric and Ocean Optics: Atmospheric Physics", 9680, 968037-1-968037-7, doi:10.1117/12.2205281, 2015b.

Smalikho, I.N., Banakh, V.A., Falits, A.V., and Rudi Yu.A.: Determination of turbulence energy dissipation rate from data measured by the Stream Line lidar in the atmospheric surface layer, Atmos. Oceanic Optics, 28(10), 980-987, DOI: 10.15372/AOO20151006, 2015a [in Russian].

Smalikho, I.N., Banakh, V.A., Holzäpfel,F., and Rahm, S.: Estimation of aircraft wake vortex parameters from the array of radial velocities measured by a coherent Doppler lidar, Atmos. Oceanic Optics, 28(8), 742-750, DOI:10.15372/AOO20150801, 2015b [in Russian].

Smalikho, I.N., Banakh, V.A., Holzäpfel, F., and Rahm, S.: Method of radial velocities for the estimation of aircraft wake vortex parameters from data measured by coherent Doppler lidar, Optics Express, 23(19), A1194-A1207, doi:10.1364/OE.23.0A1194, 2015c.

Spiridonov, Yu.G., Pichugin, A.P., and Shestopalov, V.P.: Space radar observation of atmospheric internal gravity waves, FEAS USSR, 296(2), 317-320, 1987 [in Russian].

Sun, J., Nappo, C. J., Mahrt, L., Beluši´c, D., Grisogono, B., Stauffer, D. R., Pulido, M., Staquet, C., Jiang, Q., Pouquet, A., Yagüe, C., Galperin, B., Smith, R. B., Finnigan, J. J., Mayor, S. D., Svensson, G., Grachev, A. A. and Neff, W. D.: Review of wave-turbulence interactions in the stable atmospheric boundary layer, Reviews of Geophysics, 53, 956-993, doi:10.1002/2015RG000487, 2015.

Vakkari, V., O'Connor, E.J., Nisantzi, A., Mamouri, R.E., and Hadjimitsis, D.G.: Low-level mixing height detection in coastal locations with a scanning Doppler lidar, Atmos. Meas. Tech., 8, 1875–1885, doi:10.5194/amt-8-1875-2015, 2015.

Vel'tishchev, N.F., and Stepanenko,V.M.: Mesometeorological Processes. Moscow State University Publishers, 2006 [in Russian].

Vinnichenko, N.K., Pinus, N.Z., Shmeter, S.M., and Shur G.N.: Turbulence in the Rree Atmosphere. Edit by J.A.Dutton, Consultants Bureau, 262 pp., 1973.

Wang, Y., Creegan, E., Felton, M., Ligon, D. and Huynh, G.: Investigation of nocturnal low-level jet–generated gravity waves over Oklahoma City during morning boundary layer transition period using Doppler wind lidar data, J. Appl. Remote Sens., 7(1), 1-14, doi:10.1117/1.JRS.7.073487, 2013.

Table 1. Main parameters of the HALO Photonics Stream Line lidar.

Wavelength	1.5 μm
Pulse energy	14 μJ
Pulse duration	170 ns
Pulse repetition frequency	15 kHz
Initial beam diameter (e^{-2})	5.6 cm
Focus length	$\geq$ 300 m
Telescope diameter	8 cm
Sampling frequency (length)	50 MHz (3 m)
Nyquist velocity	$\pm$ 19.5 m/s
Minimum range	90 m
Maximum range	9600 m

Table 2. Measurement parameters.

Range gate length	30 m
Number of points per range gate	10
Elevation angle	60 deg
Height resolution	26 m
Number of pulses for accumulation	3000
Integration time per ray	0.2 s
Focus length	800 m
Velocity resolution	0.0382 m/s
Scanning speed	10 deg/s
Azimuth angle resolution	2 deg
Number of rays per scan	180
Duration of one scan	36 s

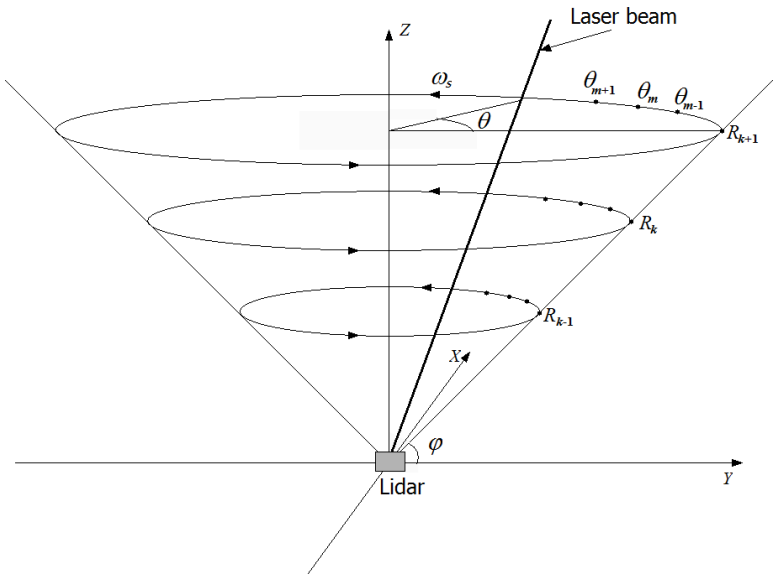

5

Figure 1: Geometry of measurement by a pulsed coherent Doppler lidar with the conical scanning by the laser beam.

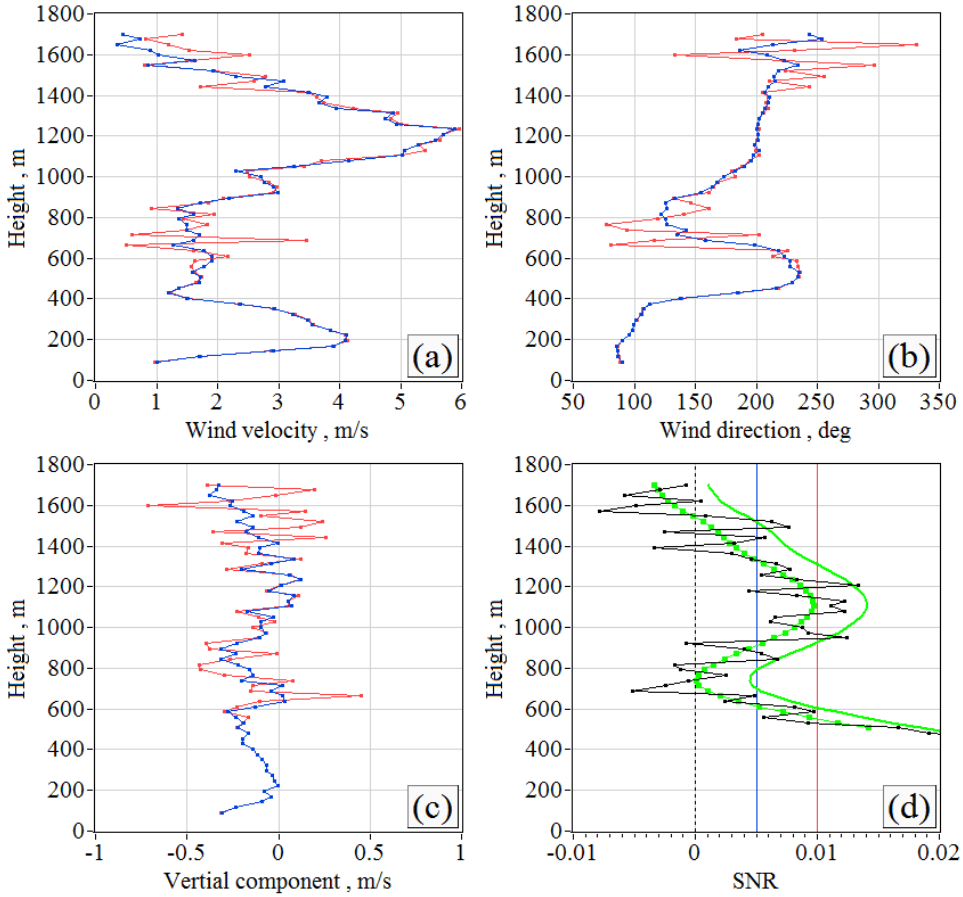

Figure 2: Height profiles of wind velocity (a), wind direction angle (b) and vertical component the wind vector (c) retrieved from data measured by the Stream Line lidar, using LSM (red curves) and FSWF (blue curves); (d): height profiles of signal-to-noise ratio estimates $\overline{\mathrm{SNR}}$ (black curve), SNR_s (green squares) and SNR_c (green solid curve).

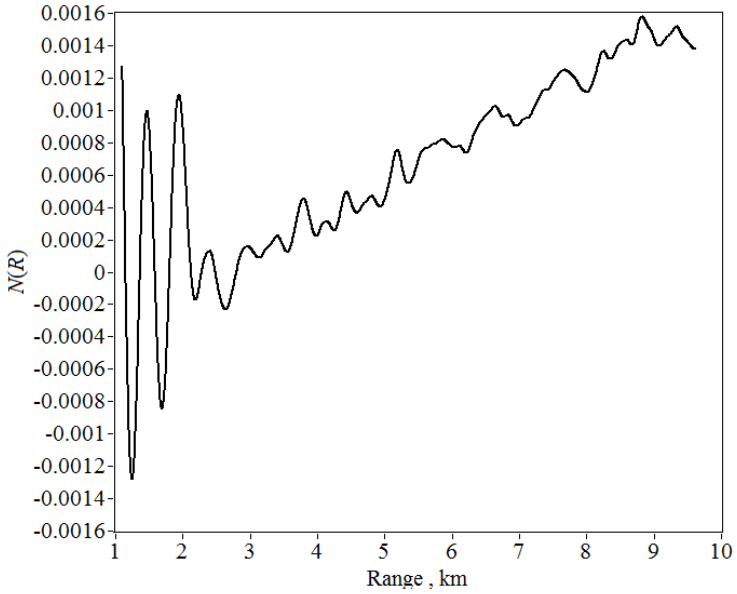

Figure 3: Function $N(R)$.

Figure 4: Map of lidar wind measurements in August 14-28 of 2015.

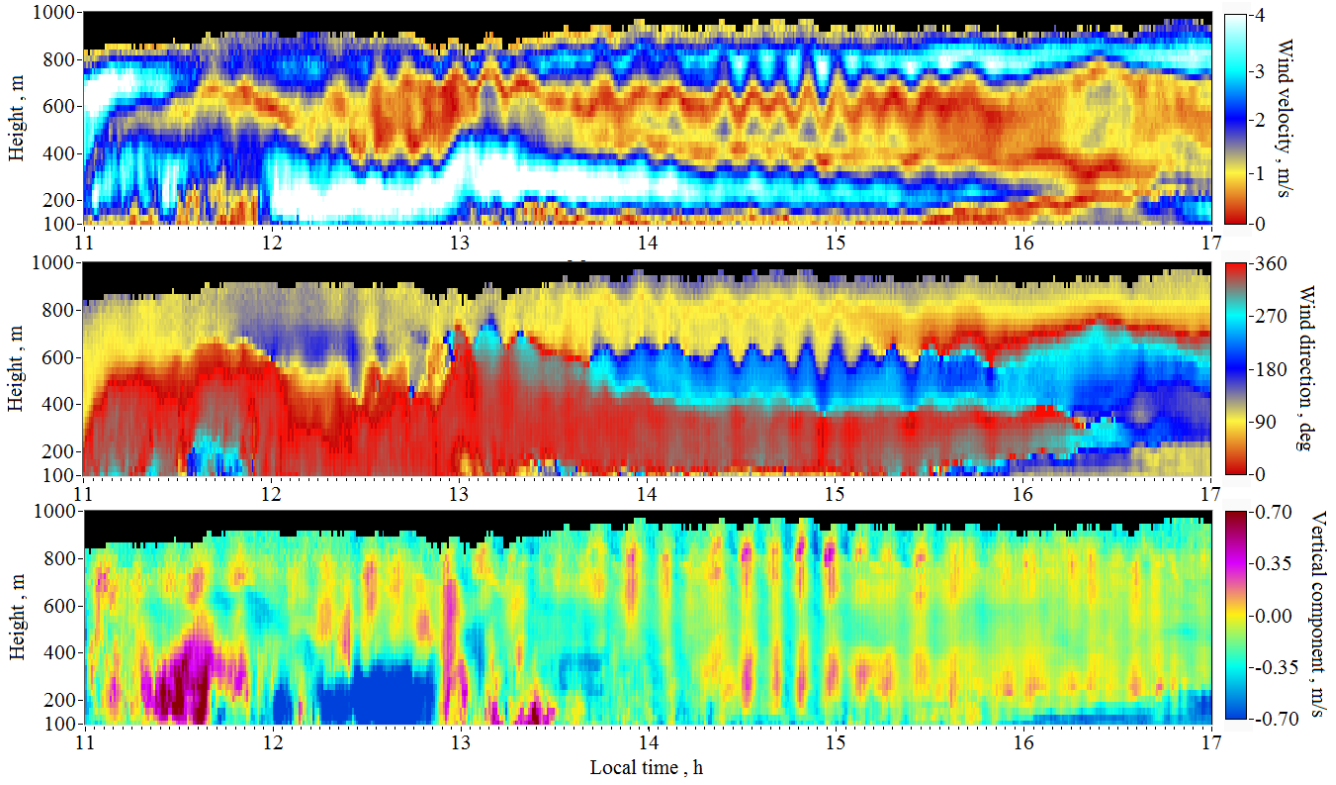

Figure 5: Spatiotemporal distributions of the wind speed (a), the wind direction angle (b), and the vertical component of the wind vector (c) obtained from measurements with the Stream Line lidar on August 23 of 2015.

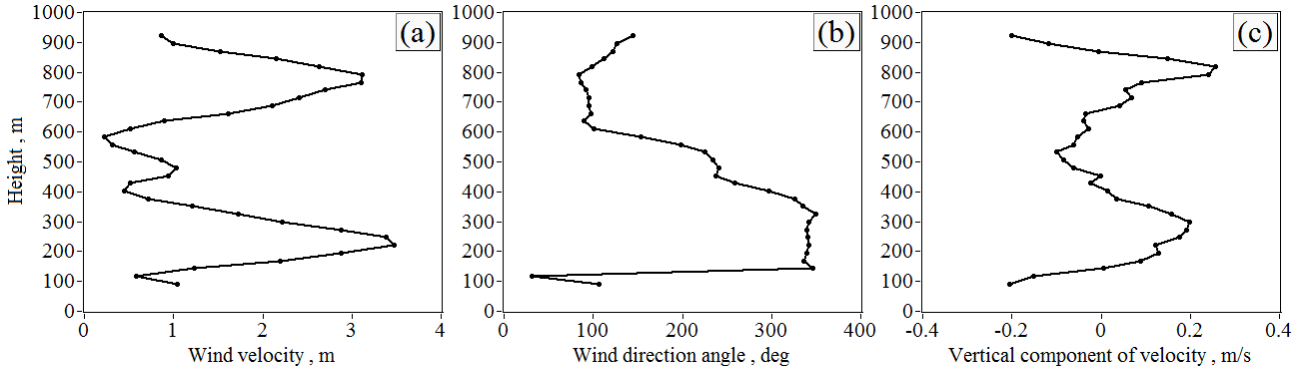

Figure 6: Vertical profiles of the wind speed (a), the wind direction angle (b), and the vertical component of the wind vector (c) taken from the data of Fig.4 (these profiles were measured at 14:31 LT).

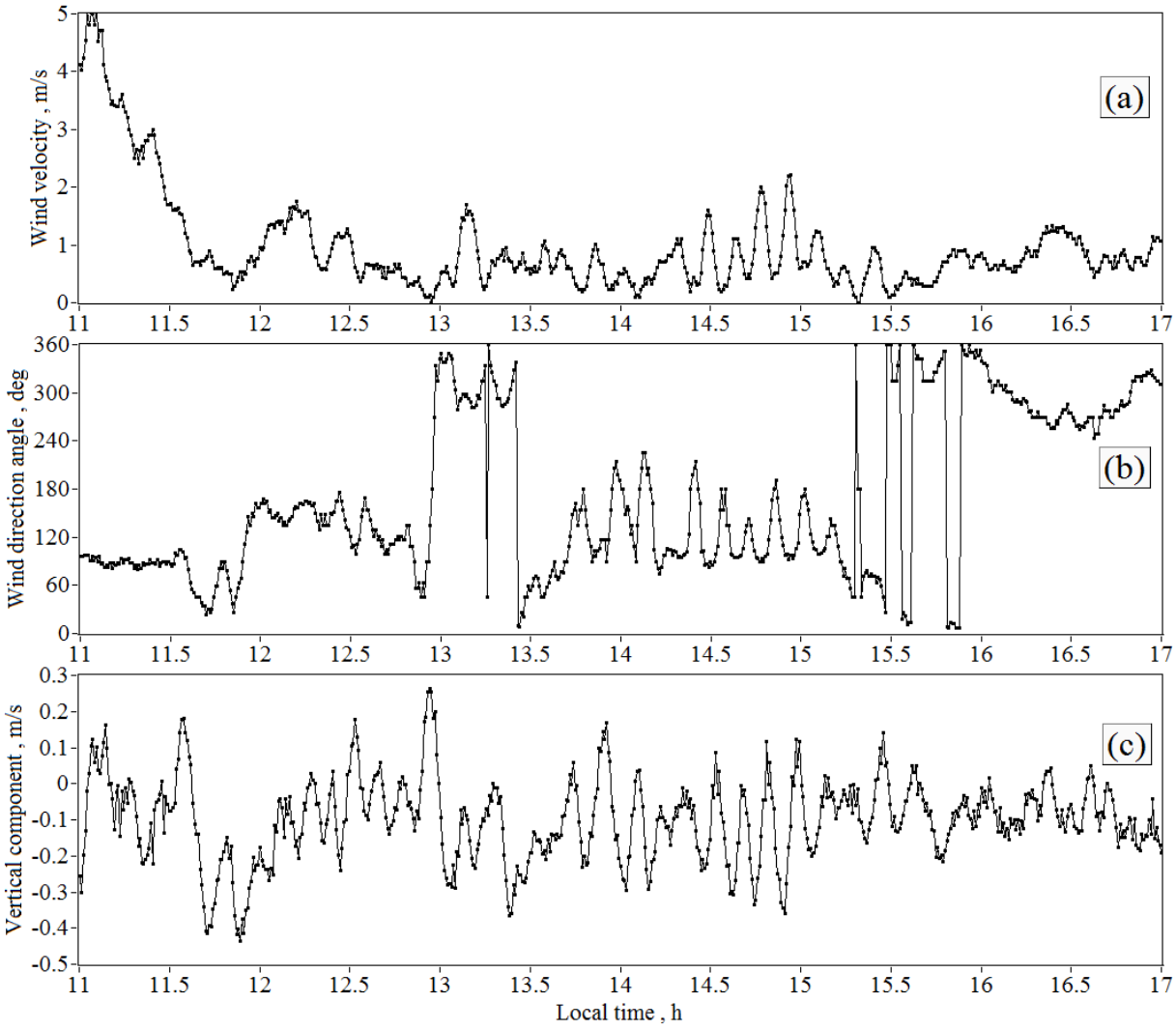

Figure 7: Temporal profiles of the wind speed (a), the wind direction angle (b), and the vertical component of the wind velocity (c) taken from the data of Fig. 5 (measurement height of 636.5 m).

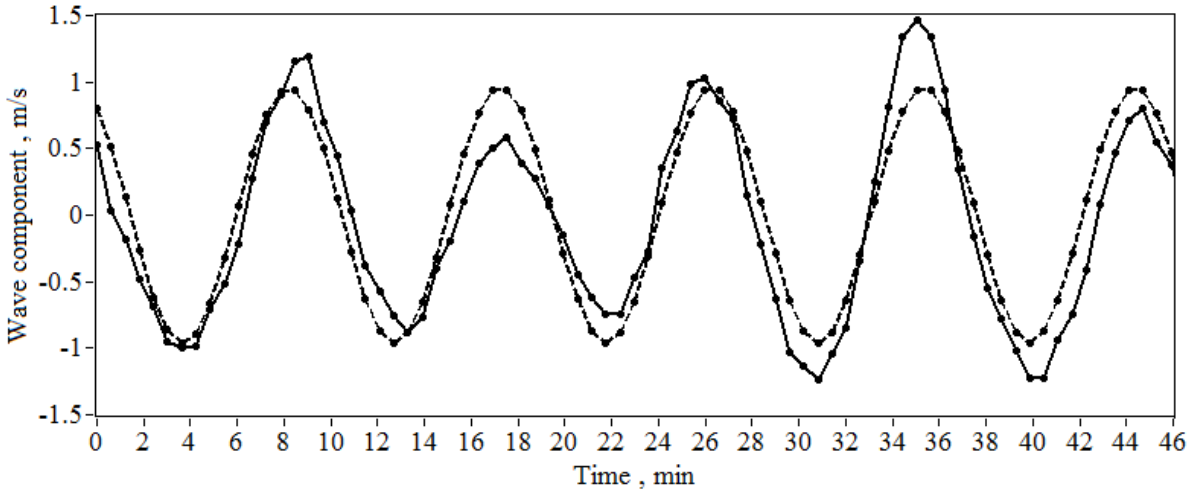

Figure 8: Time dependence of the wave addend of the longitudinal wind velocity: (solid curve) measurements by the Stream Line lidar starting from 14:20 LT on August 23 of 2015 at a height of 766.4 m AGL (the data of Fig.5(a) were used); (dashed curve) result of least-square fitting of sine-wave dependence (2) for the wave addend $\tilde{V}_x(t)$ to the measured data shown by the solid curve.

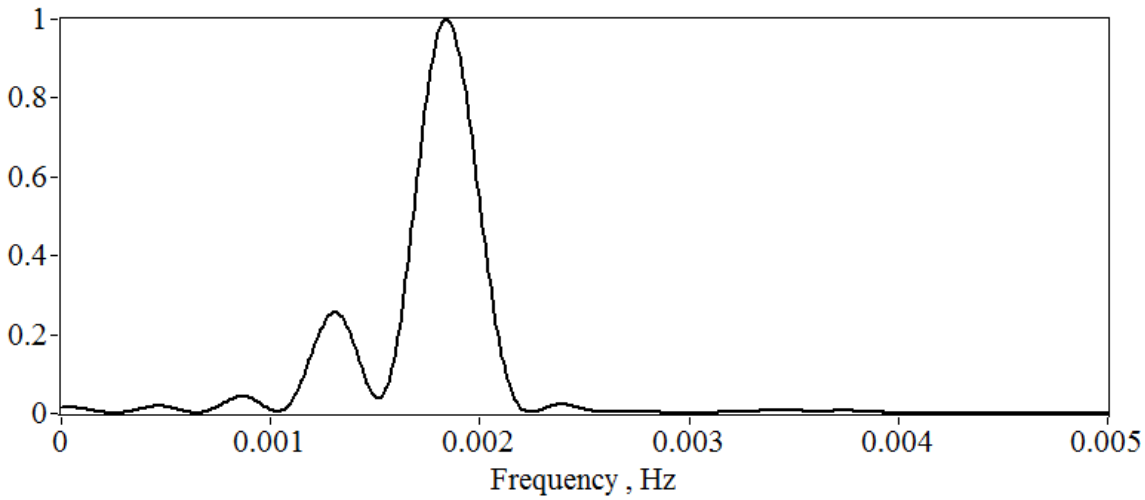

Figure 9: Normalized spectrum of the wave addend of wind velocity calculated from the data shown by the solid curve in Fig. 8.

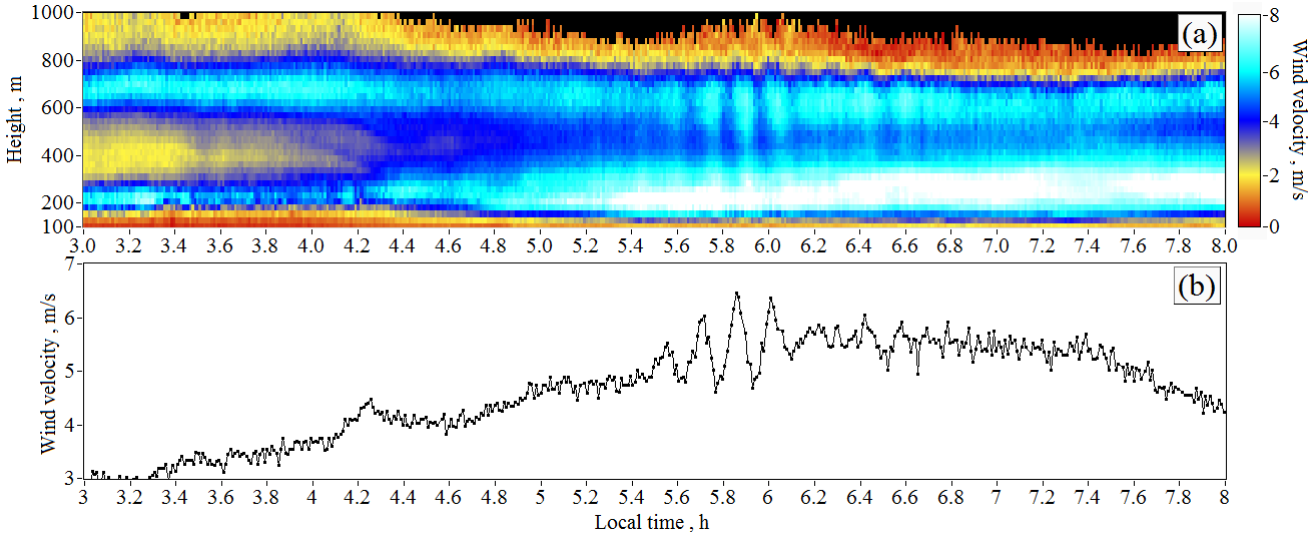

Figure 10: Spatiotemporal distribution of the wind velocity (a) and the time profile of the wind velocity at a height of 532.6 m AGL (b) obtained from measurements by the Stream Line lidar on August 20 of 2015.

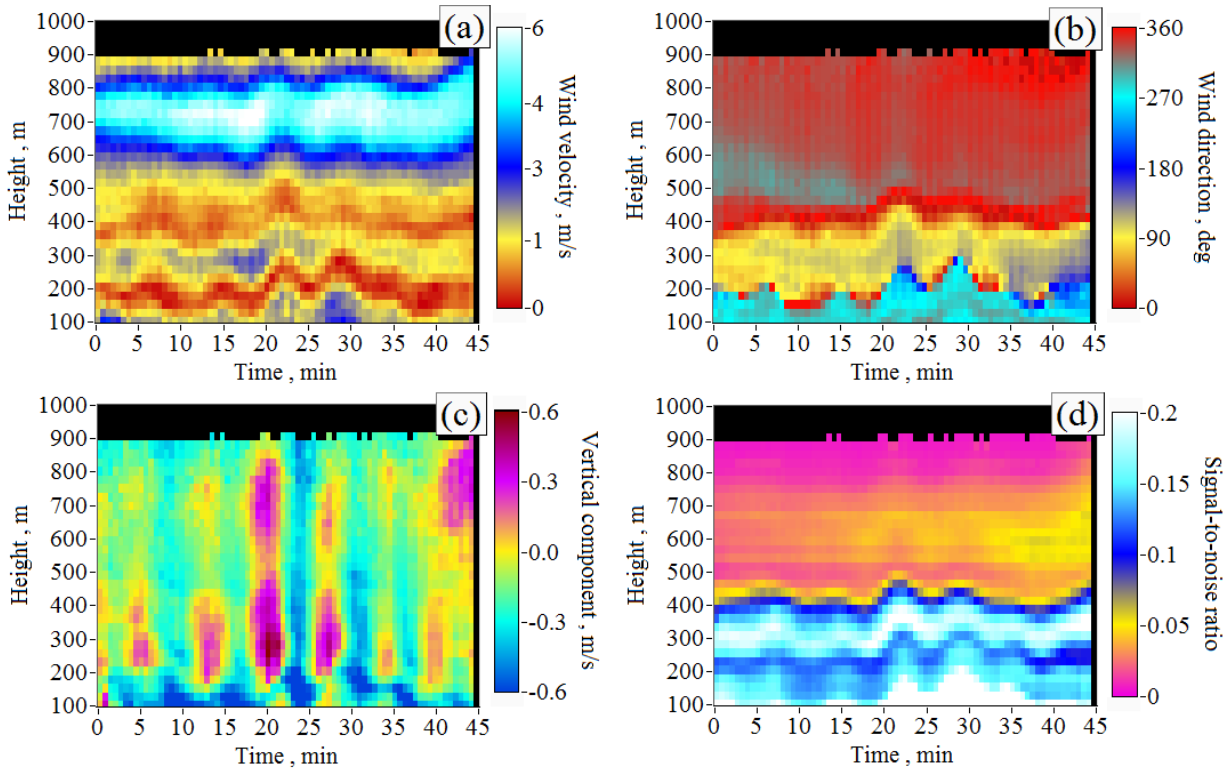

Figure 11: Spatiotemporal distributions of the wind speed (a), wind direction angle (b), vertical component of the wind vector (c), and signal-to-noise ratio (d) obtained from measurements of the Stream Line lidar on August 14 of 2015 starting from 19:24 LT.

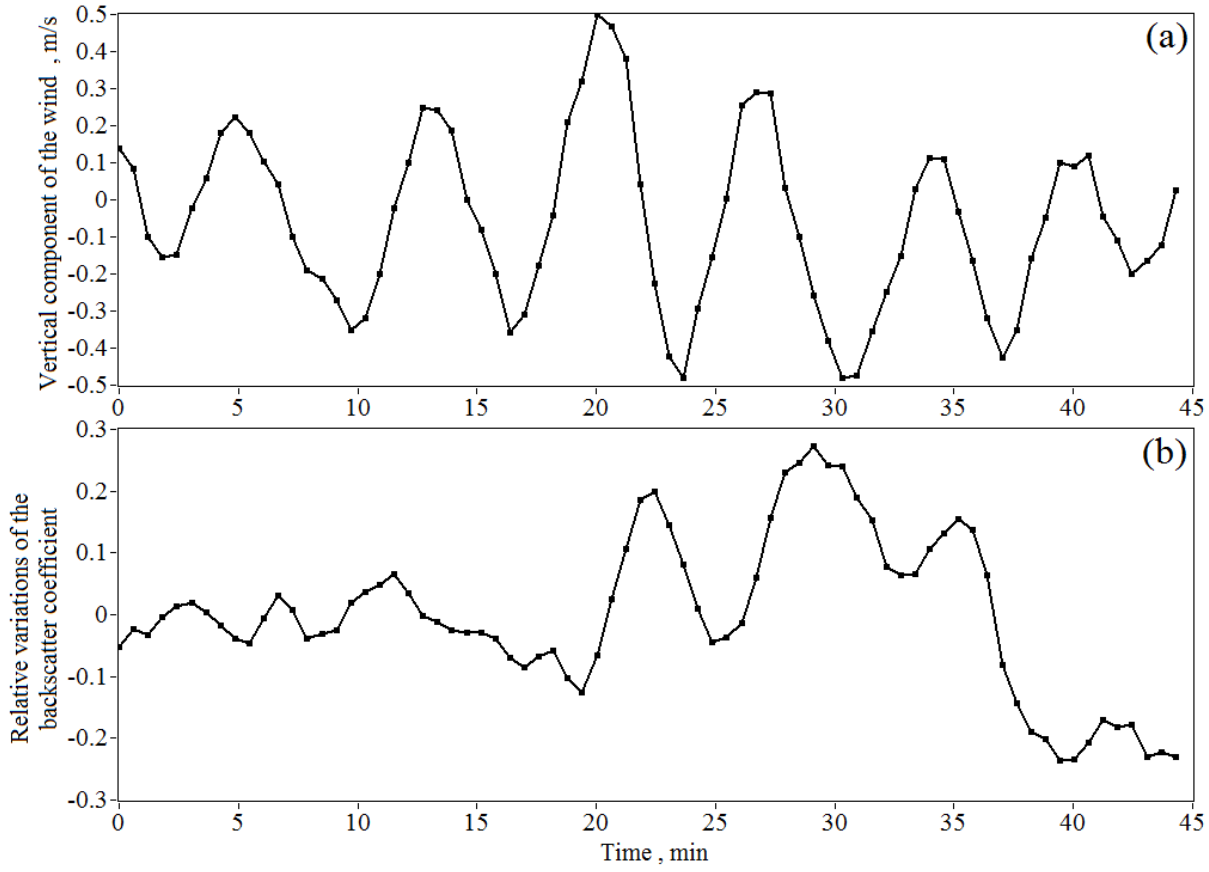

Figure 12: Time dependence of the vertical component of the wind vector (a) and relative variations of the aerosol backscatter coefficient (b) obtained from the data depicted in Fig. 11(c, d) at a height of 220.8 m AGL.